Production of medical radioisotopes ^{51}Cr, ^{62,64}Cu, and ^{99m}Tc by laser-induced photonuclear reactions*

Xuan Pang (庞萱)[1] Di Wu (吴笛)[2,3†] Bao-Hua Sun (孙保华)[1‡] Mei-Zhi Wang (王美植)[2,3] Hao-Yang Lan (蓝浩洋)[2,3]
Yu-Hui Xia (夏宇辉)[2,3] Zhe-Nan Wang (王哲男)[2,3] Xin-Lu Xu (徐新路)[2,3] Xue-Qing Yan (颜学庆)[2,3]

[1]School of Physics, Beihang University, Beijing 100191, China
[2]State Key Laboratory of Nuclear Physics and Technology, School of Physics, CAPT, Peking University, Beijing 100871, China
[3]Beijing Laser Acceleration Innovation Center, Beijing 101407, China

Abstract: Laser-driven bremsstrahlung photon sources offer a promising approach to producing medical radioisotopes by photonuclear reactions. In this work, we report new activation measurements of ^{nat}Cr, ^{nat}Cu, and ^{nat}Ru by laser-driven bremsstrahlung at Peking University's Compact Laser Plasma Accelerator laboratory. It utilized the 200 TW laser with a 0.2 Hz repetition frequency and 2-mm-thick targets. An activity of 2.27 Bq for ^{51}Cr, 5110 Bq for ^{62}Cu, 53.9 Bq for ^{64}Cu, and 16.4 Bq for ^{99m}Tc has been achieved after a 20-30 minutes' irradiation. These crucial data, together with the dedicated Monte Carlo simulations, enable a realistic evaluation to address the growing demand in nuclear medicine. It is found that utilizing a repetition frequency of 100 Hz for the 200 TW laser and 10-cm-thick targets can meet the clinical diagnostic requirements of a typical activity of MBq for the isotopes of interest.

Keywords: Medical radioisotope, Photonuclear reaction, Laser-driven bremsstrahlung, Monte-Carlo simulation

DOI: **CSTR:**

I. INTRODUCTION

Diagnostic and therapeutic procedures using radioisotopes are now routine in the field of medicine. The relevant radioisotopes are typically produced in nuclear reactors or cyclotrons. In comparison, photonuclear reactions produce less heat due to lower gamma-induced energy deposition, allowing the use of thicker targets with reduced cooling needs [1]. Furthermore, they allow simultaneous multi-target irradiation [2], maximizing γ-beam utilization for efficient production of various radioisotopes, including novel isomers [3, 4] that traditional methods cannot produce.

In recent decades, with the rapid development of high-intensity and high-repetition-frequency laser systems, photonuclear reactions using these systems have been considered a promising method for radioisotope production [5]. In laser-driven bremsstrahlung photon sources, electrons are accelerated by ultrafast laser pulses. The accelerated electrons bombard a bremsstrahlung converter, leading to photon emission and subsequent photonuclear reactions with the target material. The efficient production of radioisotopes relies on the enhancement of photonuclear cross sections in the vicinity of the giant dipole resonance (GDR), which reaches the maximum at several MeV to a few tens of MeV. The safety and miniaturization of laser systems enable the production of radioisotopes closer to hospitals, thereby reducing their loss during transportation. Moreover, the narrow focal spot of the laser confines the reaction to a small area, significantly increasing the specific activity of the radioisotope. However, the method is still in an early stage of development.

In this work, we focus on the production of four medical radioisotopes: chromium-51 (^{51}Cr), copper-62 (^{62}Cu), copper-64 (^{64}Cu), and technetium-99m (^{99m}Tc). ^{51}Cr and ^{99m}Tc are typically produced in reactors, whereas ^{62}Cu and ^{64}Cu are generated by cyclotrons. ^{51}Cr is used to label red blood cells for monitoring and to quantify loss or bleeding of gastrointestinal proteins [6–8]. ^{62}Cu is a relatively short-lived β^+ emitter that is very suitable for PET imaging [9]. The radioisotope ^{64}Cu with an appropriate half-life of 12.7 h, has a low β^+ end-point energy of 0.65 MeV, which is comparable to that of ^{18}F ($T_{1/2}$ = 110

Received 3 October 2025; Accepted 31 December 2025
* Supported by the National Natural Science Foundation of China (No. 12325506)
† E-mail: wdwd@pku.edu.cn
‡ E-mail: bhsun@buaa.edu.cn

min), the most widely used positron emitter. It emits virtually no γ-ray. On the other hand, its multiple decay modes make it suitable for combining positron emission tomography (PET) and targeted therapy [10, 11]. Moreover, ^{64}Cu can form a "matched pair" with ^{62}Cu, enabling the measurement of uptake kinetics in an organ by PET imaging and allowing for precise dosimetric calculations [12, 13]. ^{99m}Tc is an ideal radioisotope for single-photon emission computed tomography (SPECT), making it the most common radioisotope used in diagnostic procedures [14, 15]. It accounts for approximately 80% of all nuclear medicine procedures and 85% of diagnostic scans worldwide [16]. However, a large majority of reactors producing ^{99m}Tc are expected to shut down by 2030 [17].

At present, the studies using the laser-driven photonuclear reactions mainly focus on ^{62}Cu, ^{64}Cu and ^{99m}Tc, which are generated by the reaction of ^{63}Cu$(\gamma,n)^{62}$Cu, ^{65}Cu$(\gamma,n)^{64}$Cu, and ^{100}Mo$(\gamma,n)^{99}$Mo/^{99m}Tc [18, 19]. In particular, the relevant experiments have been performed at the XingGuangIII and CLAPA laser facilities [20, 21]. However, the achieved yields remain insufficient for clinical applications in humans, being adequate only for preclinical animal studies.

In this study, we aim to evaluate the yield of ^{51}Cr, ^{62,64}Cu, and ^{99m}Tc radioisotopes via laser-induced photonuclear reactions, utilizing both experimental and simulation approaches. The experimental setup and data analysis are introduced in Section II. Then the yields of these medical radioisotopes are discussed and evaluated in Section III. Finally, a summary is given in Section IV.

II. EXPERIMENT AND DATA ANALYSIS

The experiments were performed at the 200 TW laser facility in the Compact Laser Plasma Accelerator (CLAPA) Laboratory at Peking University. The schematic layout of the experimental setup is shown in Fig. 1. Electrons are generated in the laser wake field acceleration (LWFA) by focusing the laser on a supersonic nozzle. Accelerated electrons collide with a converter, producing bremsstrahlung photons that subsequently undergo photonuclear reactions with the target nuclei. During the experiment, the laser system was operated at a relatively low energy, with a delivered energy of approximately 2.4 J to the target and a full-width at half-maximum (FWHM) duration of 30 fs. The laser beam was focused to 21 μm×23 μm (FWHM) at the nozzle. The gas jet is a 4×1 mm rectangular supersonic nozzle, which can provide a flat density distribution for pure helium gas. The helium pressure is adjustable from 0 to 45 bar, and varying it can change the electron energy. A 40 μm Al foil and a 60 μm Be window are used to block scattered light and seal the vacuum, respectively. A turbo integrating current transformer (Turbo-ICT) is used to measure the electron charge. The energy spectrum of electrons is measured by a 0.8 T magnetic spectrometer located 100 cm away from the gas jet. Fluorescent screens (Gd_2O_2S:Tb) at the entrance and exit of the magnet are used in conjunction with CCD cameras to record electron signals. There is no converter or experimental target for electron beam measurement. More details about the experiment setup and the electron parameters can be found in Refs. [22, 23].

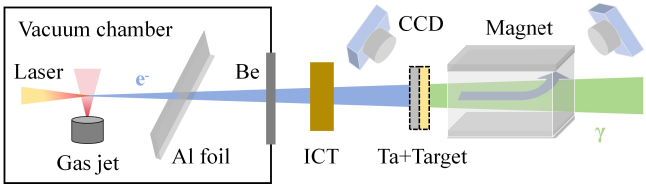

Fig. 1. (Color online) Schematic layout of experimental setup. Refer to the text for details.

In this experiment, the average electron charge per shot was 458 pC, with a peak energy of 200 MeV at gas pressures of 27 bar. The divergence angle was approximately 4.3 mrad. A Ta (99.9%) disk with a size of 2×2 cm and a thickness of 2 mm was employed as a bremsstrahlung converter. The monochromatic electron spectrum, as shown in Fig. 2, was determined using a magnetic spectrometer. It has limited acceptance, resulting in a truncated energy range up to 65 MeV. The bremsstrahlung γ-ray spectrum in Fig. 2, is obtained by the Geant4 toolkit [24−26] by taking the average electron spectrum of 100 continuous shots as input. The effect of the truncated low-energy electrons is considered to be negligible as a result of their small portion.

The natural chromium (^{nat}Cr), copper (^{nat}Cu), and ruthenium (^{nat}Ru) targets have the same size as the Ta converter and are placed next to the converter. The relevant data on the medical radioisotopes produced are shown

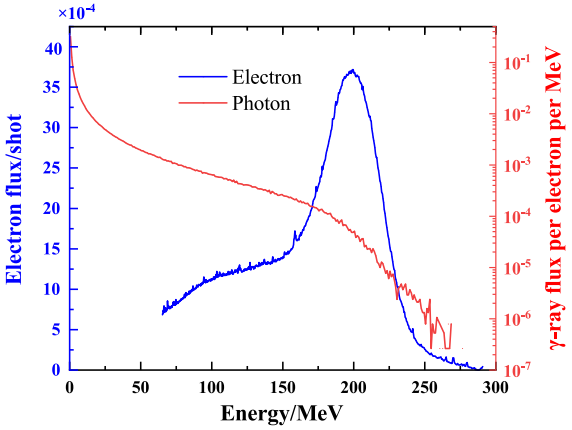

Fig. 2. (Color online) The monochromatic electron spectrum measured by the magnetic spectrometer (blue line) and bremsstrahlung γ-ray spectrum per electron simulated by Geant4 toolkit [24−26] (red line).

in Table 1. The repetition frequency was set at 0.2 Hz to maintain the acceptable vacuum. ^{nat}Cu was irradiated for 20 min with approximately 241 laser shots. The irradiation time of ^{nat}Cr and ^{nat}Ru was 30 min, with about 361 laser shots per target. It took about 10 min to transfer the target to the offline measurement after irradiation.

The characteristic γ-ray spectra after irradiation were measured using two HPGe detectors with a relative efficiency of 40% (relative to the NaI(Tl) detector) and a 3×3 inch $LaBr_3$ detector. All detectors are placed in a low-background measurement system. The detector efficiencies were calibrated with standard ^{152}Eu and ^{60}Co sources. The summing coincidence correction was determined by Monte Carlo simulations [30], based on the actual geometry of the background detection system. The total offline measurement time was approximately 28 h for ^{nat}Cu and 24 h for ^{nat}Ru. For ^{nat}Cr target, offline measurements were performed a total of 7 times within 60 days after irradiation, each with a duration of 16–40 h. As shown in Fig. 3, three characteristic peaks at energies of 320.1 keV, 511 keV and 140.5 keV from the decay of ^{51}Cr, ^{62,64}Cu and ^{99m}Tc are well distinguished. The peaks of the background spectrum in Fig. 3(a) and Fig. 3(c) are rooted in the decays of actinides in the environment. The broad-energy continuum of bremsstrahlung enables the simultaneous activation of multiple photonuclear reaction channels. Apart from the contribution of ^{62,64}Cu, ^{60,61}Cu can also induce β^+ decay and then emit 511 keV γ-rays. The cross sections of photoneutron reactions that generate these Cu isotopes are shown in Fig. 4. The ^{63}Cu$(\gamma,2n)$ reaction is the dominant source of ^{61}Cu, whereas the cross sections for other reaction channels producing ^{60,61}Cu are both significantly smaller (< 0.5 mb). Compared with the half-life of ^{64}Cu ($T_{1/2}$ = 12.70 h), the shorter half-lives of ^{61}Cu (3.34 h) and ^{60}Cu (23.74 min) ensure their complete decay within approximately 15 hours after irradiation. Therefore, they do not interfere with the subsequent decay measurement of ^{64}Cu. For ^{62}Cu ($T_{1/2}$ = 9.67 min), within five half-lives of its decay, the contribution of 511 keV γ-rays originating from ^{60,61}Cu accounts for only about 1%, which is negligible within the statistical uncertainties.

Based on the energy spectra measured at different time periods, the activity at time t can be calculated as follows:

$$A(t) = \frac{\lambda \Delta N e^{-\lambda t}}{e^{-\lambda t} - e^{-\lambda(t+\Delta T)}}, \tag{1}$$

where ΔN is the characteristic peak counts after background subtractions within the measurement time ΔT. The initial activity A_0 of the radioisotope can be deduced by an exponential fit to the $A(t)$. In Fig. 3(b), both the decays of ^{62}Cu and ^{64}Cu contribute to the 511 keV peak. The initial activities can be determined using double-exponential fitting, given their very different half-lives. The corresponding compounds are displayed in Fig. 3(d). The steep beginning of the curve is mainly due to the rapid decay of ^{62}Cu, while the flat part is mainly attributed to the slow decay of ^{64}Cu. The activity at the initial time $t = 0$ in Fig. 3(d) corresponds to the activity at the end of irradiation.

For laser-driven γ-rays with low repetition frequencies, the total yield N of the product at the end of irradiation can be derived using the following equation:

$$N = \sum_{i=1}^{n} Y_i \exp(-\lambda(n-i)/f), \tag{2}$$

where n is the total shots, λ is the decay constant of the reaction product, f is the repetition frequency and Y_i represents the yield of the i-th shot. The experimental results are summarized in Table 2. The experimental single-shot yield is calculated as the total yield divided by the number of shots. The total uncertainty includes uncertainties in statistical fluctuations, calibration of the detection efficiency, the half-life and decay branching ratio, and γ-ray absorption in the target. The γ-ray absorption in targets has also been corrected. With a repetition frequency of

Table 1. The decay properties of medical radioisotope ^{51}Cr, ^{62,64}Cu, ^{99m}Tc and information of the corresponding photonuclear reaction. The first column represents the target in the photonuclear reaction. The natural abundance of the target is denoted as *Abu.*. The third column indicates the type of photonuclear reactions. The produced medical radioisotopes are characterized by the half-lives $T_{1/2}$ and decay modes. Here, $\%\varepsilon$ represents the probabilities of nuclear decay via electron capture or β^+ decay. $\%IT$ represents the probabilities of nuclear decay via isomeric transitions. And the characteristic γ-ray energy in the decay, as well as the branching ratio intensity, are also provided. The last column indicates whether experimental data for the photonuclear reaction cross section are available in the EXFOR database [27]. The data are obtained from Ref. [28].

Target isotope	*Abu.* (%)	Reaction	Product	$T_{1/2}$	Decay mode	γ-ray energy	Intensity	EXFOR data
^{52}Cr	83.79%	(γ,n)	^{51}Cr	27.70 d	$\%\varepsilon = 100$	320.1 keV	10%	Yes
^{63}Cu	69.15%	(γ,n)	^{62}Cu	9.67 min	$\%\varepsilon = 100$	511 keV	196%	Yes
^{65}Cu	30.85%	(γ,n)	^{64}Cu	12.70 h	$\%\varepsilon = 61.5$	511 keV	35%	Yes
^{100}Ru	12.60%	(γ,p)	^{99m}Tc	6.01 h	$\%IT = 99.99$	140.5 keV	89%	No

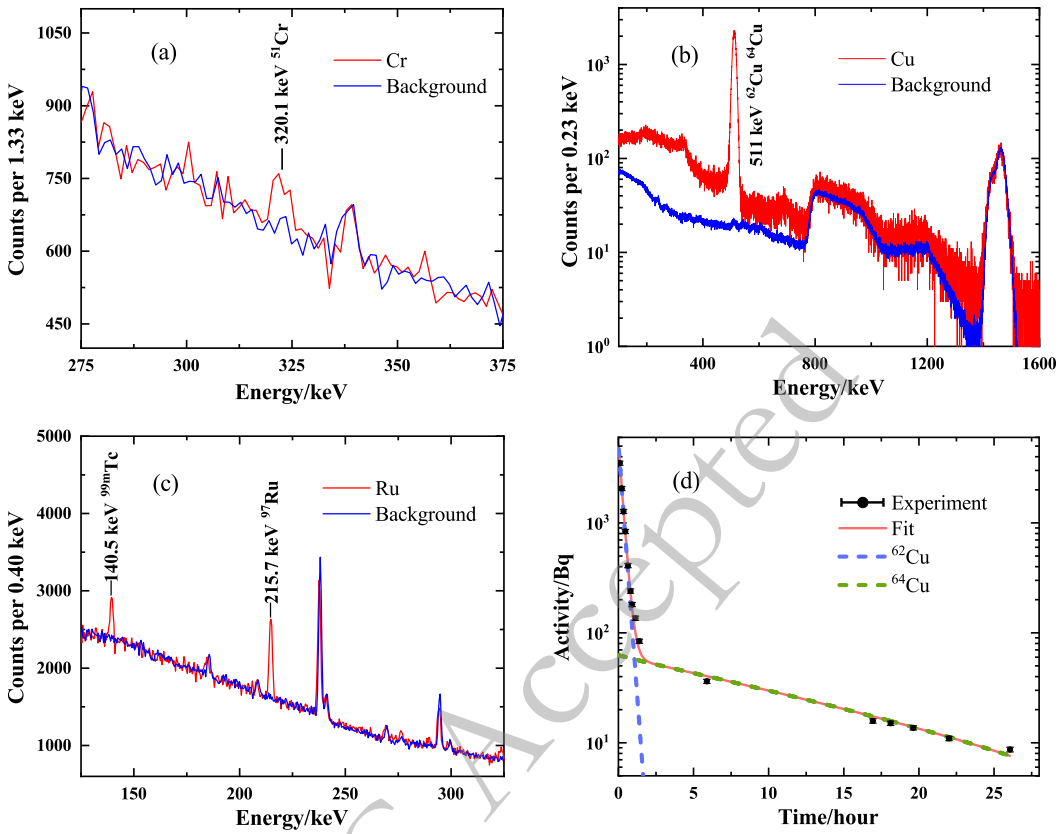

Fig. 3. (Color online) Energy spectra of the irradiated ^{nat}Cr target (a), the ^{nat}Cu target (b), and the ^{nat}Ru target (c). The measurement times for spectra (a), (b), and (c) are 16.16 h, 287.26 s and 12.24 h, respectively. The activity curve of ^{nat}Cu (d) is contributed by ^{62}Cu and ^{64}Cu. The energy spectra for ^{nat}Cr and ^{nat}Ru are measured using a HPGe detector, while the energy spectrum for ^{nat}Cu is obtained with a $LaBr_3$ detector. The background spectra are normalized by the measurement time and shown in panels (a)~(c).

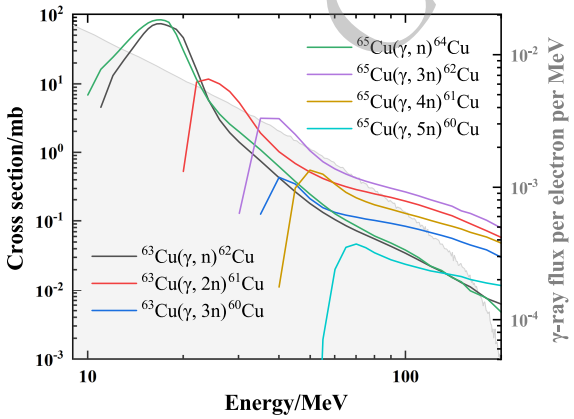

Fig. 4. (Color online) The cross sections of photoneutron reactions for ^{63,65}Cu. The data are derived from the TENDL-2023 library [29, 31]. The grey area represents the bremsstrahlung spectrum as shown by the red line in Fig. 2.

0.2 Hz, irradiation of 2-mm-thick natural targets for 20 min yields activities of 5110 Bq for ^{62}Cu and 53.9 Bq for ^{64}Cu, while for 30 min yields activities of 2.27 Bq for ^{51}Cr and 16.4 Bq for ^{99m}Tc. Although the experimental results demonstrate the viability of producing medical radioisotopes via laser-driven bremsstrahlung sources, the achieved activity is much lower than that required for clinical applications (MBq~GBq).

III. SIMULATION AND EVALUATION

Various parameters, such as electron current, number of shots, converter, and target size, limit the yield of medical radioisotopes via laser-induced photonuclear reactions. To optimize the production system, we performed the Monte Carlo simulations using the Geant4 version 11.0.3 toolkit [24−26]. The precision of the simulation is constrained by the available nuclear data, with the photonuclear reaction cross section being the key factor. Cross-section data are essential for determining the optimal energy range, predicting radioisotope yields, and estimating impurity levels. In Geant4, the cross sections for photonuclear reactions can be provided by the G4GammaNuclearXS (G4GNXS), G4PhotoNuclearCrossSection (G4PNCS), or the LEND model. However, the photonuclear reaction cross sections obtained by the G4GNXS and G4PNCS classes are notably inconsistent with the existing experimental data [32]. Although the LEND model is in good agreement with the experimental data, it can only

Table 2. The experimental and simulated results of the irradiated 2-mm-thick Cr, Cu, and Tc natural target. The third and fourth columns show the experimentally measured activity and the resulting single-shot yield for a target thickness of 2 mm. The fourth and fifth columns represent the experimental single-shot yield calculated by dividing the total yield by the number of shots, and the simulated single-shot yield from the Monte Carlo with the same irradiated conditions, respectively. The last column indicates the evaluated single-shot results in the simulation with a target thickness of 10 cm. In the simulations, the photonuclear reaction cross sections are taken from the TENDL-2023 library [29].

Irradiated target	Product	Exp. activity (Bq)	Single-shot yield	Sim. single-shot yield	Eval. single-shot yield
^{nat}Cr	^{51}Cr	2.27±0.16	(2.49±0.18)×10^{4}	2.78×10^{4}	8.47×10^{5}
^{nat}Cu	^{62}Cu	(5.11±0.21)×10^{3}	(2.95±0.12)×10^{4}	4.18×10^{4}	9.44×10^{5}
	^{64}Cu	53.9±4.8	(1.07±0.09)×10^{4}	1.28×10^{4}	2.89×10^{5}
^{nat}Ru	^{99m}Tc	16.4±1.4	(1.71±0.14)×10^{3}	2.15×10^{3}	6.50×10^{4}

provide data with energies below 20 MeV. At present, there are serious challenges in data scarcity and data quality on photonuclear reactions, particularly for the (γ, p) reaction channel.

The TENDL-2023 library [29, 31] is established as one of the references in nuclear data libraries. The library is based on both default and adjusted TALYS calculations [33] and is used worldwide for the analysis and prediction of nuclear reactions. In this work, we adapted the TENDL-2023 library into Geant4 using the Geant4-GENBOD toolkit [32]. The simulation algorithm is detailed in Ref. [34].

Table 2 presents the simulated and evaluated results of the single-shot yield. Under the same experimental conditions, the simulated single-shot yield agrees with experimental data within a factor of 1.5. The observed discrepancies may arise from shot-to-shot instabilities in laser acceleration and from differences between the cross sections in the TENDL-2023 library used in Geant4 and the actual photonuclear cross sections. In the evaluated case, a natural target thickness of 10 cm is used. Compared with thin targets, one must account for secondary reactions from Compton scattering and attenuation of gamma rays within the target. The wide spectrum of bremsstrahlung enables the simultaneous opening of multiple reaction channels. Table 3 summarizes the ratio of single-shot yield between the major byproduct isotopes and the desired medical radioisotope under the evaluated case, providing reference data for future applications. Although the yields of isotopes with different atomic numbers are relatively high, they can be readily separated via chemical methods [35−37]. For ^{nat}Ru, the yield of ^{99m}Tc is much lower than that of other byproducts. Therefore, using enriched ^{100}Ru targets could be considered to increase the yield in future production.

Fig. 5 illustrates the relationship between product activity and repetition frequency. The irradiated time is three times the half-life of the products. After three half-lives of irradiation, the activity of the product has reached 88% of its saturation value. The grey area indicates the activity levels of ^{62}Cu and ^{64}Cu required for PET imaging

Table 3. The ratio of single-shot yield between the major byproduct isotopes and the desired medical radioisotope (^{51}Cr for ^{nat}Cr, ^{62,64}Cu for ^{nat}Cu, and ^{99m}Tc for ^{nat}Ru) in the simulation with a natural target thickness of 10 cm. Specifically, the ratio is relative to ^{62}Cu in the case of ^{nat}Cu. The produced isotope is characterized by the half-life $T_{1/2}$.

Target	Isotope	$T_{1/2}$	Ratio (%)
^{nat}Cr	^{48}Cr	21.56 h	0.26
	^{49}Cr	42.3 min	5.26
	^{49}V	330 d	11.44
	^{50}V	stable	11.86
	^{51}V	stable	70.01
^{nat}Cu	^{61}Cu	3.34 h	7.77
	^{61}Ni	stable	13.86
	^{62}Ni	stable	51.38
	^{63}Ni	100.80 y	0.65
	^{64}Ni	stable	12.35
^{nat}Ru	^{93}Tc	2.78 h	3×10^{2}
	^{94}Tc	293 min	7×10^{2}
	^{95}Tc	19.26 h	4.6×10^{3}
	^{97}Tc	4.21×10^{6} y	5.3×10^{3}
	^{95}Ru	1.61 h	7.2×10^{3}
	^{97}Ru	2.84 d	6.3×10^{3}
	^{103}Ru	39.25 d	1.34×10^{4}

[38, 39]. For the production of ^{62}Cu, a lower frequency (~600 Hz) is sufficient to meet the standards for PET imaging. With a half-life of 9.67 min for ^{62}Cu, its saturation activity is achieved within one hour in Fig. 6. ^{64}Cu is also a promising radionuclide for targeted radiotherapy, with a recommended therapeutic dose of 99 MBq/kg [40]. For a standard adult patient (60 kg), this corresponds to approximately 6 GBq of administered activity. However, as shown in Fig. 6, the saturated activity is not sufficient to meet the requirements of this clinical therapy.

Red blood cells radiolabeled with ^{51}Cr are used to

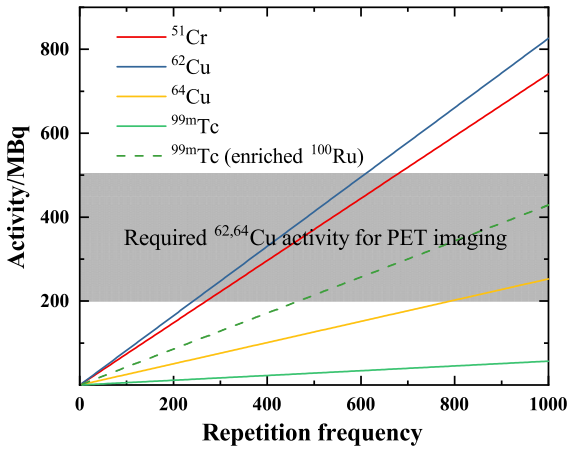

Fig. 5. (Color online) Activity (in the unit of MBq) of ^{51}Cr, ^{62,64}Cu, and ^{99m}Tc versus repetition frequency (in the unit of Hz). The irradiated time is three times the half-life of radioisotopes. The grey area shows the required activities for PET imaging. All the solid lines represent the expected activities from the relevant targets. The dotted line represents the available activity of ^{99m}Tc when using a 95% enriched ^{100}Ru target.

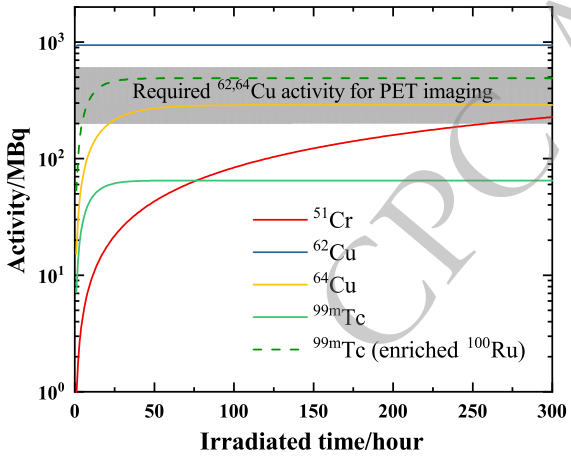

Fig. 6. (Color online) Same as Fig. 5 but as a function of irradiation time (in hours). The repetition frequency is set to 1 kHz.

identify hemolytic anemia. In a clinical case, 4.07 MBq of ^{51}Cr-sodium chromic was used [8]. As shown in Fig. 6, it is sufficient to irradiate for only 20 hours to reach the required level for a clinical trial.

^{99m}Tc is a commonly used imaging agent for SPECT imaging. The required activity varies depending on the purpose of clinical treatment. Brain perfusion imaging typically employs activities of 555–1110 MBq, with 740 MBq serving as the standard [41]. For bone scintigraphy in adults, the average activity administered by a single intravenous injection should be 500 MBq (300–740 MBq) [42]. Myocardial perfusion imaging uses an administered activity of 500 MBq for a standard examination [43]. In contrast, pulmonary perfusion scintigraphy employs a reduced activity of 200 MBq [44]. Currently, its saturation activity is approximately 65 MBq. When employing a 95% enriched ^{100}Ru target, the achievable activity of ^{99m}Tc can reach 500 MBq. Furthermore, the required activity level for SPECT imaging can be attained either by utilizing multiple synchronized lasers or by increasing the repetition frequency.

IV. SUMMARY

In this study, we performed the activation measurements using the 200 TW laser facility at the CLAPA laboratory. The natural Cr, Cu, and Ru targets were irradiated for 20-30 minutes with a 0.2 Hz repetition frequency. We obtain the activity of 2.27 Bq for ^{51}Cr, 5110 Bq for ^{62}Cu, 53.9 Bq for ^{64}Cu, and 16.4 Bq for ^{99m}Tc. However, the achieved activity is far from being suitable for clinical usage. To bridge this gap, we evaluated potential production by simulations employing the cross sections from the TENDL-2023 library. With a natural target thickness of 10 cm and a frequency of several hundred Hz, the simulated results can reach several 100 MBq for ^{51}Cr and ^{62,64}Cu, meeting clinical application requirements. For ^{99m}Tc, employing a 95% enriched ^{100}Ru target, the activity can reach 500 MBq, which is sufficient for clinical SPECT imaging.

Currently, the stable and continuous operation of a kilohertz laser-plasma accelerator has been reported [45]. However, the peak energy of the electron bunches is only 2.5 MeV, which results in a bremsstrahlung source with photon energies substantially below the (γ,n) and (γ,p) reaction thresholds for most nuclei. At high peak power levels, such as 200 TW in the CLAPA laboratory, increasing the repetition frequency poses significant challenges to the thermal resistance and damage of laser gain medium and mirror materials. Additionally, maintaining electron beam stability remains a critical issue. Another type of laser-driven gamma source, which employs the laser Compton scattering (LCS) technology, may have the potential to produce medical radioisotopes at a clinical scale [46, 47]. For example, the newly built Shanghai Laser Electronic Gamma Source (SLEGS) [48, 49] and the upcoming Extreme Light Infrastructure – Nuclear Physics facility (ELI-NP) [50].

References

[1] D. Habs and U. Köster, Appl. Phys. B **103**, 501 (2011)
[2] Y. X. Yang, W. J. Zhao, X. G. Cao, *et al.*, Radiat. Phys. Chem. **218**, 111599 (2024)
[3] H. Y. Lan, D. Wu, J. X. Liu, *et al.*, Nucl. Sci. Tech. **34**, 74

(2023)
[4] W. T. Pan, T. Song, H. Y. Lan, *et al*., Appl. Radiat. Isot. **168**, 109534 (2021)
[5] Z. L. Sun, AIP Advances **11**, 040701 (2021)
[6] A. Freud, A. Canfi, and E. Ben-Hur, Int. J. Radiat. Biol. **63**, 651 (1993)
[7] D. M. Mock, G. L. Lankford, J. A. Widness, *et al*., Transfusion **39**, 156 (1999)
[8] B. W. Audrey and V. G. Vesper, J. Nucl. Med. Technol. **36**, 95 (2008)
[9] P. J. Blower, J. S. Lewis, and J. Zweit, Nucl. Med. Biol. **23**, 957 (1996)
[10] X. K. Sun and C. J. Anderson, Method Enzymol. **386**, 237 (2004)
[11] C. J. Anderson and R. Ferdani, Cancer Biother. Radiopharm. **24**, 379 (2009)
[12] A. Bockisch, J. Nucl. Med. Mol. Imaging **38**, 1 (2011)
[13] S. M. Qaim, B. Scholten, and B. Neumaier, J. Radioanal. Nucl. Chem. **318**, 1493 (2018)
[14] S. Banerjee, M. R. Ambikalmajan Pillai, and N. Ramamoorthy, Semin. Nucl. Med. **31**, 260 (2001)
[15] A. Duatti, Nucl. Med. Biol. **92**, 202 (2021)
[16] "World Nuclear Association, Radioisotopes in Medicine," retrieved 10th September 2024.
[17] *IAEA Annual Report for 2021*, Tech. Rep. (IAEA, 2022).
[18] A. D. Roberts, C. G. R. Geddes, N. Matlis, *et al*., Appl. Radiat. Isot. **96**, 122 (2015)
[19] Z. G. Ma, H. Y. Lan, W. Y. Liu, *et al*., Matter Radiat. Extremes **4**, 064401 (2019)
[20] Z. W. Cao, W. Qi, H. Y. Lan, *et al*., Plasma Phys. Control. Fusion **65**, 055007 (2023)
[21] J. Y. Zhang, D. Wu, H. Y. Lan, *et al*., Nucl. Sci. Tech. 35 (2024), 10.1007/s41365-024-01550-x.
[22] D. Wu, H. Y. Lan, J. Y. Zhang, *et al*., arXiv: 2209.13947 [nuclex].
[23] M. Z. Wang, D. Wu, H. Y. Lan, *et al*., Nucl. Phys. A **1043**, 122834 (2024)
[24] S. Agostinelli, J. Allison, K. Amako, *et al*., Nucl. Instrum. Methods A **506**, 250 (2003)
[25] J. Allison, K. Amako, J. Apostolakis, *et al*., IEEE Tran. Nucl. Sci. **53**, 270 (2006)
[26] J. Allison, K. Amako, J. Apostolakis, *et al*., Nucl. Instrum. Methods A **835**, 186 (2016)
[27] "Experimental Nuclear Reaction Data (EXFOR)," retrieved 23th September 2024.
[28] "NuDat 3 database," retrieved 23th September 2024.
[29] A. J. Koning and D. Rochman, Nucl. Data Sheets **113**, 2841 (2012)
[30] L. C. He, L. J. Diao, B. H. Sun, *et al*., Nucl. Instrum. Methods A **880**, 22 (2018)
[31] A. J. Koning, D. Rochman, J. Sublet, *et al*., Nucl. Data Sheets **155**, 1 (2019)
[32] W. Luo, H. Y. Lan, Y. Xu, *et al*., Nucl. Instrum. Methods Phys. Res. A **849**, 49 (2017)
[33] A. J. Koning, S. Hilaire, and S. Goriely, Eur. Phys. J. A **59**, 131 (2023)
[34] W. Luo, M. Bobeica, I. Gheorghe, *et al*., Appl. Phys. B **122**, 8 (2016)
[35] B. Y. Wu, C. P. Liu, C. Y. Fu, *et al*., Chem. Eng. J. **373**, 1030 (2019)
[36] Y. Xue, Y. X. Hua, J. J. Ru, *et al*., Adv. Powder Technol. **32**, 2791 (2021)
[37] S. Uchida and K. Tagami, Anal. Chim. Acta **357**, 1 (1997)
[38] T. Z. Wong, J. L. Lacy, N. A. Petry, *et al*., Am. J. Roentgenol. **190**, 427 (2008)
[39] T. Zhang, S. K. Das, D. R. Fels, *et al*., Am. J. Roentgenol. **201**, W698 (2013)
[40] K. Ito, Y. Narita, M. Hiroki, *et al*., J. Nucl. Med. **66**, 2510946 (2025)
[41] Ö. L. Kapucu, F. Nobili, A. Varrone, *et al*., Eur. J. Nucl. Med. Mol. Imaging **36**, 2093 (2009)
[42] T. Van den Wyngaert, K. Strobel, W. U. Kampen, *et al*., Eur. J. Nucl. Med. Mol. Imaging **43**, 1723 (2016)
[43] H. J. Verberne, W. Acampa, C. Anagnostopoulos, *et al*., Eur. J. Nucl. Med. Mol. Imaging **42**, 1929 (2015)
[44] *Guideline on core SmPC and package leaflet for technetium (^{99m}Tc) macrosalb*, Tech. Rep. (Committee for Medicinal Products for Human Use, 2016).
[45] L. Rovige, J. Huijts, I. Andriyash, *et al*., Phys. Rev. Accel. Beams **23**, 093401 (2020)
[46] Y. N. Gu, W. J. Zhao, X. G. Cao, *et al*., Nucl. Sci. Tech. **35**, 155 (2024)
[47] X. Pang, B. H. Sun, L. H. Zhu, *et al*., Nucl. Sci. Tech. **34**, 187 (2023)
[48] H. W. Wang, G. T. Fan, W. Q. Shen, *et al*., Nucl. Phys. News **33**, 17 (2023)
[49] H. W. Wang, G. T. Fan, L. X. Liu, *et al*., Nucl. Sci. Tech. **33**, 87 (2022)
[50] D. Filipescu, A. Anzalone, D. L. Balabanski, *et al*., Eur. Phys. J. A **51**, 185 (2015)